Lab on a Chip

Accepted Manuscript

Volume 1 | Number 1 | Jan 2013 | Pages 1–100

Lab on a Chip

Miniaturisation for chemistry, physics, biology, materials science and bioengineering

www.rsc.org/loc

ROYAL SOCIETY OF CHEMISTRY

ROYAL SOCIETY OF CHEMISTRY

www.rsc.org/loc

Towards ultra-high peak capacities and peak-production rates using spatial three-dimensional liquid chromatography

Bert Wouters[1], Ekaterina Davydova[2], Sam Wouters[1], Gabriel Vivo-Truyols[2], Peter J. Schoenmakers[2], Sebastiaan Eeltink[1*]

[1]Vrije Universiteit Brussel, Department of Chemical Engineering, Pleinlaan 2, B-1050 Brussels, Belgium

[2]Universiteit van Amsterdam, Van 't Hoff Institute for Molecular Sciences, Science Park 904, 1098 XH Amsterdam, The Netherlands

(*) corresponding author
Pleinlaan 2, B-1050, Brussels, Belgium
Tel.: +32 (0)2 629 3324, Fax: +32 (0)2 629 3248, E-mail: seeltink@vub.ac.be

Abstract

In order to successfully tackle the truly complex separation problems arising from areas such as proteomics research, the development of ultra-efficient and fast separation technology is required. In spatial three-dimensional chromatography, components are separated in the space domain with each peak being characterized by its coordinates in a three-dimensional separation body. Spatial three-dimensional (3D-)LC has the potential to offer unprecedented resolving power when orthogonal retention mechanisms are applied, since the total peak capacity is the product of the three individual peak capacities. Due to parallel developments during the second- and third-dimension separations, the analysis time is greatly reduced compared to a coupled-column multi-dimensional LC approach. This communication discusses the different design aspects to create a microfluidic chip for spatial 3D-LC. The use of physical barriers to confine the flow between the individual developments, and flow control by the use of ^{2}D and ^{3}D flow distributors is discussed. Furthermore, the *in-situ* synthesis of monolithic stationary phases is demonstrated. Finally, the potential performance of a spatial 3D-LC systems is compared with the performance obtained with state-of-the-art 1D-LC and (coupled-column) 2D-LC approaches via a Pareto-optimization approach. The proposed microfluidic device for 3D-LC featuring 16 ^{2}D channels and 256 ^{3}D channels can potentially yield a peak capacity of 8,000 in a total analysis time of 10 minutes.

Keywords: Multi-dimensional LC separations; 3D-LC; Spatial chromatography; Proteomics, Pareto optimization

1. Introduction

Analytical techniques hyphenated with mass-spectrometry, such as high-performance liquid chromatography – mass spectrometry (HPLC–MS), have become indispensable tools for biomarker-discovery studies.[1] As proteins are key components in biological processes, proteomic studies are of utmost importance for the discovery of disease biomarkers.[2] In biofluids such as human plasma, both the large number of analytes (tens of thousands of different proteins) and their enormous dynamic concentration range (up to ten orders of magnitude) pose a huge analytical challenge.[3] To reduce spectral complexity and to minimize ion-suppression effects, high-efficiency separations are required prior to mass-spectrometric analysis. However, current HPLC–MS approaches, including two-dimensional LC strategies, cannot provide the resolution required for the identification and quantification of all constituents present in the truly complex samples encountered in life-science research.[4] Hence, the development of novel separation technology is required to achieve ultra-high peak capacities within a reasonable time, allowing the analysis of a multitude of samples.

Three-dimensional liquid-chromatographic (3D-LC) separations may offer ultra-high peak capacities, given that the total peak capacity is the product of the three individual peak capacities provided that orthogonal retention mechanisms are achieved.[5] In 1995, Jorgenson *et al*. demonstrated the potential of a column-based online 3D-LC (^{T}LC×^{T}LC×^{T}CE) separation for peptides, by coupling size-exclusion chromatography (SEC), reversed-phase (RP-)LC, and a capillary zone electrophoresis (CZE) approach.[6] The individual peak capacities were estimated to be 5 (SEC), 23 (RP-LC), and 24 (CZE), respectively, yielding a total estimated peak capacity of 2800 in a total analysis time of 6 hours. In a recent study, Davydova *et al.* concluded that by adding a third dimension separation, a two-fold gain in peak capacity could be obtained, compared to conventional ^{T}LC×^{T}LC separations using two coupled columns.[7]

As an alternative to a column-based approach, three-dimensional separations can be performed by analyte migration to different positions in a three-dimensional separation body (^{X}LC×^{X}LC×^{X}LC), which extends in three directions (X, Y, Z) in space.[8] After completing the ^{1}D development (X axis), all fractions are developed in parallel in the ^{2}D separation (X-Y plane). Finally, all ^{2}D fractions are developed in parallel in a ^{3}D separation (Z axis). Due to parallel ^{2}D and ^{3}D developments of all obtained fractions, the analysis time can be greatly reduced compared to a column-based ^{T}LC×^{T}LC×^{T}LC approach. However, major challenges that need to be addressed before such technology can be realized include confinement and flow control in the three subsequent individual developments and the implementation of suitable stationary phases providing orthogonal retention mechanisms.[8] Because components are separated in space, rather than in time, detectors with a spatial resolution should be applied for *in-situ* detection, such as confocal imaging techniques. Alternatively, it is possible to perform the third dimension in time, so as not to retain the separated components in the three-dimensional separation body, but to elute them in the last dimension ($^{X}LC\times^{X}LC\times^{T}LC$). This implies that the components are spatially resolved in the first and second dimension, but temporally resolved in the third dimension.

This study concerns the design aspects for the construction of a microfluidic device for comprehensive spatial three-dimensional liquid chromatography ($^{X}LC\times^{X}LC\times^{T}LC$). A first prototype of the device is presented. The use of physical barriers to confine the flow between the ^{1}D and ^{2}D developments, and the use of ^{2}D and ^{3}D flow distributors is demonstrated. Furthermore, the *in-situ* synthesis of a macroporous methacrylate-ester-based monolithic stationary phase is demonstrated. Finally, the potential of spatial three-dimensional chromatography is discussed in terms of peak capacity and analysis time in comparison with state-of-the-art 1D-^{T}LC and (coupled-column) 2D-^{T}LC approaches using a Pareto-optimization approach.[9]

2. Theory

A Pareto-optimization approach was applied to calculate the potential performance in terms of peak capacity (n_c) and analysis time (t_ω) for protein separations with 1D-^{T}LC, 2D-^{T}LC, and $^{X}LC\times^{X}LC\times^{T}LC$ systems. The Pareto-optimality approach relies on the ability to find a single expression that relates all the objectives of the optimization.[9] When this expression is found, the so-called Pareto front can be defined, which corresponds to those experimental conditions in which it is not possible to improve one objective without worsening the other(s). When this approach is applied to system optimization in n-dimensional chromatography, at least two objectives arise, *i.e.*, (maximum) peak capacity (n_c) and (minimum) analysis time (t_ω). In order to obtain an expression that relates both objectives, the plate-height equation and the pressure-drop equation have to be combined. The reduced van-Deemter plate-height equation has been used to relate the reduced plate height ($h = H/d_{dom}$) to the reduced mobile-phase velocity ($\nu = u_0 \cdot d_{dom}/D_m$):

$$h = a + \frac{b}{\nu} + c \cdot \nu \qquad (1)$$

where a, b, and c represent the reduced eddy-diffusion, longitudinal-diffusion and resistance-to-mass-transfer parameters, respectively. For all systems the use of a polymer-monolithic stationary phase for the gradient separations of proteins was assumed. Therefore, equal plate characteristics (a, b, c) were applied for the 1D, 2D, and 3D-LC separations, see Table I. The domain size (d_{dom}) is defined as the sum of the macropore and polymer microglobule size.[10] The pressure drop across the column/channel length (L) is governed by Darcy's law, according to:

$$\Delta P = \frac{u_0 \cdot \phi \cdot \eta \cdot L}{d_{dom}^2} \tag{2}$$

where ϕ is the flow resistance, u_0 the mobile-phase velocity of an unretained component, and η the mobile-phase viscosity. For the column-based ^{T}LC and ^{T}LC×^{T}LC systems, the maximum operating pressure was kept constant at 100 MPa, *i.e.*, ultra-high-pressure conditions. The maximum pressure drop for ^{X}LC×^{X}LC×^{T}LC systems was fixed at 2 MPa. The equation that links the total analysis time (t_ω) in gradient-elution mode with the column dead time (t_0) and gradient time (t_G) is:

$$t_0 = \frac{t_\omega}{\frac{t_G}{t_0} + 1} \tag{3}$$

where the approximation $t_\omega = t_G + t_0$ is implicit. Both objectives (t_ω and n_c) are connected via Darcy's and Van Deemter equations. We start with the connection between t_ω and t_0 via Eq. 3, in which the parameter t_G/t_0 is optimized. As $L = u_0 \cdot t_0$, a connection between t_ω and L/u_0 is obtained. To calculate and compare the performance limits of 1D-^{T}LC, 2D-^{T}LC, and ^{X}LC×^{X}LC×^{T}LC systems we have considered ΔP, ϕ, η as fixed parameters (in order to reduce the complexity of the calculations) and d_{dom} and L as variable parameters to optimize. Table I summarizes the values of parameters that were fixed and provides all variables and corresponding ranges in which they were optimized. Next, a given value of t_ω defines a single pair of values of u_0 and L, which in turn provide a single plate-height value via Eq. 1. In a last step, H can be related to the peak capacity (n_c).

In conventional time-based one-dimensional gradient liquid chromatography (1D-^{T}LC), the peak capacity (${}^{1}n_c$) is defined as:[11]

$${}^{1}n_c = \frac{t_G}{t_0} \cdot \frac{\sqrt{L}}{4 \cdot R_s \cdot (1 + k_e) \cdot \sqrt{H}} + 1 \tag{4}$$

where R_s the resolution (R_s = 1), and k_e the retention factor at the moment of elution which depends on the gradient steepness factor ($S \cdot \Delta\varphi$), and can be estimated by:[12]

$$k_e = \frac{t_G}{t_0} \cdot \frac{1}{S \cdot \Delta\varphi} \qquad (5)$$

In a time-based two-dimensional gradient ^{T}LC×^{T}LC system, the total peak capacity ($^{2}n_c$) can be calculated as the product of the peak capacities of each dimension, assuming the use of orthogonal retention mechanisms in the two dimensions:[7]

$$^{2}n_c = \frac{^{1}t_G}{4 \cdot R_S \cdot \sqrt{\dfrac{\left(^{1}k_e + 1\right)^2}{\dfrac{L_1}{H_1}} \cdot \dfrac{^{1}t_\omega^2}{\left(\dfrac{^{1}t_G}{t_0} + 1\right)^2} + \dfrac{^{2}t_\omega^2}{\delta_{det}^2}}} \times \frac{^{2}t_G}{4 \cdot R_S \cdot \sqrt{\dfrac{\left(^{2}k_e + 1\right)^2}{\dfrac{L_2}{H_2}} \cdot \dfrac{^{2}t_\omega^2}{\left(\dfrac{^{2}t_G}{t_0} + 1\right)^2} + \left(\dfrac{1}{FF}\right)^2 \left(\dfrac{^{1}F}{^{2}F} \cdot \dfrac{^{2}t_\omega}{\delta_{inj}}\right)^2}} \qquad (6)$$

where δ_{det}^2 and δ_{inj}^2 are the parameters that take into account low frequency of detection (in the first dimension) and injection band-broadening effects (in the second dimension). No focusing effect was considered between the subsequent developments, hence the focusing factor (FF) was fixed at 1. F is the flow rate, which can be determined as:

$$F = \left(\frac{d_c}{2}\right)^2 \cdot \frac{\pi \cdot \varepsilon_T \cdot L}{t_0} \qquad (7)$$

where d_c is the column diameter and ε_T the total porosity. The second-dimension column diameter ($^{2}d_c$) was considered twice as large as the first-dimension column diameter ($^{1}d_c$).

To calculate the Pareto front for a spatial three-dimensional device, we have extended the peak-capacity equation for spatial ^{X}LC×^{X}LC derived by Guiochon *et al.*[13] The total peak capacity of the spatial three-dimensional device ($^{3}n_c$) was calculated according to:

$$^{3}n_c = \frac{\sqrt{L_3}}{16 \cdot H^{5/2} \cdot \left(1 + \dfrac{1}{2.3 \cdot \dfrac{t_G}{t_0 \cdot S \cdot \Delta\varphi}}\right)} \cdot \frac{t_G}{t_0} \cdot \left(\sqrt{L \cdot H + \frac{\alpha^2}{12}} - \sqrt{\frac{\alpha^2}{12}}\right)^2 \qquad (8)$$

Eq. 8. takes into account a spatial 3D-LC device containing a discrete number of ^{2}D and ^{3}D channels, and the peaks are eluted from the third dimension, hence the ^{3}D step of the elution corresponds to time-based chromatography.

It is important to note that the Pareto fronts calculated for the multi-dimensional separations represents the maximum (theoretical) peak capacity that can be achieved assuming the use of orthogonal retention mechanisms in the subsequent developments.

Table I. Parameters and their (range of) variables used to calculate the Pareto-optimal fronts for 1D-^{T}LC, coupled-column 2D-^{T}LC, and spatial 3D-LC.

Name	Value	Units
Resolution, R_s	1	
Domain size, d_{dom}	2, 2.5, 3	µm
Total porosity, ε_T	0.509	
Bed tortuosity, γ	0.75	
Flow-resistance factor, ϕ	700	
Mobile-phase viscosity, η	0.001	Pa·s
Diffusion coefficient, D_m	10^{-10}	m^2/s
Reduced eddy-dispersion contribution, a	1.5	
Reduced longitudinal-diffusion contribution, b	1	
Reduced mass transfer contribution, c	0.15	
Maximum pressure drop for ^{T}LC and ^{T}LC×^{T}LC, ΔP	100	MPa
Gradient duration for ^{T}LC, first-dimension ^{T}LC×^{T}LC and ^{X}LC×^{X}LC×^{T}LC, $^{1}t_G/t_0$	5-30	
Gradient duration for second-dimension ^{T}LC×^{T}LC and ^{X}LC×^{X}LC×^{T}LC, $^{2}t_G/t_0$	1-10	
Gradient steepness factor, $S{\cdot}\Delta\varphi$	30	
Retention time of the last-eluting compound in second dimension for ^{T}LC×^{T}LC, $^{2}t_{\omega}$	0.1-4	min
Column-diameter ratio for ^{T}LC×^{T}LC, $^{1}d_c/^{2}d_c$	1:2	
Focusing factor, FF	1	
Parameter taking into account low detection frequency (in the first dimension), δ_{det}^{2}	4.76	
Parameter taking takes into account injection band broadening (in the second dimension), δ_{inj}^{2}	4	
Maximum pressure drop for ^{X}LC×^{X}LC×^{T}LC, ΔP	2	MPa
Gradient duration third dimension for ^{X}LC×^{X}LC×^{T}LC, $^{3}t_G/t_0$	1-10	
Cross section ^{1}D channel for ^{X}LC×^{X}LC×^{T}LC	1×1*	mm
Cross section ^{2}D channel for ^{X}LC×^{X}LC×^{T}LC	0.5×0.5*	mm
Diameter ^{3}D channels for ^{X}LC×^{X}LC×^{T}LC	0.5*	mm
Length ^{1}D channel for ^{X}LC×^{X}LC×^{T}LC	29*	mm
Length ^{2}D channel for ^{X}LC×^{X}LC×^{T}LC	29*	mm
Length ^{3}D channel for ^{X}LC×^{X}LC×^{T}LC	3*	mm

* Denotes the parameters for the constructed spatial microfluidic 3D-LC device depicted in Fig. 1D.

3. Experimental

3.1 Chemicals and materials

2,2′-Azobis(2-methylpropionitrile) (AIBN, 98%), Butyl methacrylate (BMA, 99%), ethylene dimethacrylate (EDMA, 98%), 1,4-butanediol (99%), 1-propanol (99.9%), were purchased from Sigma-Aldrich (Zwijndrecht, The Netherlands). Red 40 dye was purchased from Kroger (Virginia, USA). 2-propanol (Technical) was purchased from VWR (Leuven, Belgium). BMA and EDMA were purified by passing the liquids through a bed of activated alumina, to remove inhibitors. Topas COC substrate material (grade 8007) was purchased from Kunststoff-Zentrum (Leipzig, Germany)

3.2 Chip fabrication

Different channel layouts were designed in AutoCAD (Autodesk, San Rafael, CA, USA) and micromachined with a micromilling robot (Datron M7 Compact, Mühltal-Traisa, Germany). After cleaning each plate with 2-propanol the individual plates were sequentially bonded together via solvent-vapor-assisted bonding. Therefore, each plate was exposed to cyclohexane vapor for 7.5 minutes, aligned with the next plate of the stack, and pressed together for 60 minutes by applying a force of 2.5 kN. To visualize flow patterns (using concentrated Red 40 dye dissolved in 50:50 v% water:2-propanol) in the 3D flow distributor, a smaller stack of 3 plates was created using the same procedure. Images were recorded using a 1.4 Megapixel GC1380C high-resolution CCD camera from Allied Vision Technologies (Munich, Germany). This setup was also used to capture images of the bonded chip sectioned in half. To connect the microfluidic device to LC instrumentation, an aluminium holder was created, compatible with flat-bottom nanoport connections (Upchurch Scientific, Oak Harbor, USA) for 360 µm o.d. capillary fused-silica tubing.

A polymer-monolithic stationary phase was prepared *in-situ* in the confines of the 3D-LC chip via thermal polymerization of a precursor mixture based on 24 wt% BMA, 16 wt% EDMA, 26 wt% 1,4-butanediol, 34 wt% 1-propanol, and AIBN (1 wt% of total monomer content). The chip was placed in a custom-made holder and after filling the chip with the polymerization precursor mixture, the polymerization reaction was initiated with UV light (365 nm) and continued for 30 min. Finally, the device was flushed with MeOH to remove any unreacted monomers and the porogen.

3.4 Scanning electron microscopy

Bonded microfluidic devices were cut into 3 mm x 3 mm sized sections using the micromilling robot. The slices were then sputtered with a 6 nm layer of gold to reduce charging of the non-conductive material. Scanning electron micrographs of the slices were obtained by SEM in secondary-electron-imaging mode, using a JSM-IT300 by JEOL (Tokyo, Japan), operated at an acceleration voltage of 10 keV.

4 Results and discussion

4.1 Design aspects of a microfluidic device for spatial 3D-LC

The prototype microfluidic chip for spatial 3D-LC is composed of three modules, each with their own functionality and specific channel layout, see Fig. 1. Cyclic olefin copolymer (COC) has been selected as substrate materials for its high chemical resistance, good optical properties in the UV range allowing for the *in-situ* synthesis of polymer-monolithic stationary phases, and the possibility to bond different chip substrates via solvent-vapor-assisted bonding.[14] The top module of spatial 3D-LC chips features a fractal 3D flow distributor (Fig. 1A), which is connected to the middle module containing the *'downcomers'* of the 3D flow distributor and the ^{1}D separation channel with a cross-section of 1 × 1 × 42 mm (w × h × l), see Fig. 1B. The bottom module contains a ^{2}D flow distributor, 16 parallel ^{2}D separation channels (0.5 × 0.5 × 29 mm) with 16 through holes in each channel, a 2D flow collector, and 256 parallel ^{3}D channels (0.5 × 3 mm; i.d. × l), see Fig. 1C. A photograph of the prototype chip for spatial 3D-LC is depicted in Fig. 1D, with the three layers/modules irreversibly bonded via solvent-vapor-assisted bonding.

The *in-situ* synthesis of the macroporous polymer-monolithic stationary phase was based on the free-radical polymerization of mono- and divinylic monomers (BMA and EDMA) in the presence of a binary porogen (1,4 butanediol/1-propanol). Previously we demonstrated localized monolith synthesis in the ^{2}D channels of spatial 2D-LC chip using photomasking.[15] The cross-section of the spatial 3D-LC chip depicted in Fig. 2A shows the presence of the poly(butyl-*co*-ethylene dimethacrylate) monolith situated only in the channels of the 3D flow distributor, 2D flow distributor (and collector), parallel ^{2}D channels, and the ^{3}D channels. Fig. 2C shows a scanning electron micrographs of the outlet of a third dimension separation channel (that was cut in half). In the magnifications (Fig. 2D-E) the typical interconnected macroporous structure of the monolith is observed featuring 2-3 µm polymer microglobules clusters. The monolithic stationary phase appears to be well attached to the COC chip surface.

Migration of analytes is ideally confined to one dimension during each of the three stages in order to maximize the separation space. To confine the flow during the ^{1}D development with minimal dispersion to other channels, the ^{1}D separation channel was micromachined in the bottom of the middle substrate and the 2D flow distributor and the parallel ^{2}D channels in the bottom substrate, see the view of a cross-sectioned chip (Fig. 2A) and the zoom-in (Fig. 2B). Due to the difference in cross-sectional area between the ^{1}D channel, and the through holes connecting to the ^{2}D channels and 2D flow distributor, a preferential flow path is established. To simultaneously feed the parallel ^{2}D channels, a radially-interconnected 2D flow distributor was designed composed of two ordered arrays of diamond-shaped pillars orientated perpendicular to the main flow direction, see Fig. 1C. The first array of pillars distributed the ^{2}D mobile phase from a point injection across the full width of the chip, whereas the aspect ratio of the second array of diamond-shaped pillars was reduced, in order to match the number of flow distributor outlets with the 16 ^{2}D inlets. Increasing the number outlets by using smaller aspect-ratio pillars and integration of funneling wedges at the interface between the ^{1}D and ^{2}D channels prevented the presence of poorly-permeated flow zones.[15] Each of 16 ^{2}D channels contains 16 through holes spaced evenly across the channel length. The flow for the ^{3}D development is introduced via a fractal 3D flow distributor that should direct analytes situated in the X-Y plane (in the 16 parallel ^{2}D channels) to the 3D separation body (Z direction). The design of the fractal 3D flow distributor is based on tree-like pore networks initiated by earlier work concerning the modeling of biological systems, such as the vascular and respiratory systems and geomorphological systems such as river basins.[16-18] An initial design of the fractal 3D flow was composed of two substrate layers allowing the generation of eight successive generations of T-bifurcations, indexed from 0 to 8, resulting in 256 outlets. Fig. 3 shows the distribution of flow in the fractal 3D distributor. The first layer is fed from the top by an inlet channel (index 0), which splits perpendicularly in two channels (index 1), which each again split in two channels (index 2). These first two generations of T-bifurcations form an elementary cell, which is reproduced at a smaller scale for the following generations. After five generations of T-bifurcations in the same plane (see Fig. 3A), vertical ‘downcomers’ connect the first layer of the distributor with the second layer, containing the final three generations (see Fig. 3B). In the final prototype design, as depicted in Fig. 1A, an improved one-layered flow distributor is presented, omitting a bonding step.

4.2 Performance comparison: 1D-^{T}LC *versus* ^{T}LC×^{T}LC *versus* ^{X}LC×^{X}LC×^{T}LC

Fig. 4 shows the Pareto-optimal fronts calculated for protein separations using a one-dimensional ^{T}LC system, a two-dimensional ^{T}LC×^{T}LC system (using coupled columns), and a three-dimensional ^{X}LC×^{X}LC×^{T}LC system consisting of a monolithic cubic separation body, *i.e.*, without discrete ^{2}D and ^{3}D channels. The lower (left) part of each front corresponds to systems with short column lengths operated in the C-term region of the van-Deemter curve using steep gradients, while the upper (right) part of each curve corresponds to systems using longer columns/channels that are operated in the B-term region. For the one-dimensional ^{T}LC system, an increase in peak capacity is observed, but this increase levelled off for longer analysis times reaching a value of 470 after 60 minutes. These predictions are in good agreement with peak capacity values reported in literature for gradient separations of proteins on polymer-monolithic stationary phases[19], validating the magnitude of the reduced van-Deemter a, b, and c parameters and flow resistance for the polymer-monolithic column (Table I) applied for the Pareto-optimization calculations. The performance that can be achieved with the ^{T}LC×^{T}LC system is significantly better than that for 1D-^{T}LC, since the peak capacities in both orthogonal developments can be multiplied, *i.e.* $^1n_c = 342$ *versus* $^2n_c = 2021$ (factor 6) for a total analysis time of 30 min. For the ^{X}LC×^{X}LC×^{T}LC system, a Pareto-optimal value of the (maximum theoretical) peak capacity of approximately 98,370, assuming orthogonal retention mechanisms, was calculated for an analysis time of 30 min. This implies a 209-fold and 50-fold improvement in peak capacity in comparison with the one-dimensional ^{T}LC and two-dimensional ^{T}LC×^{T}LC systems, respectively. For fast separations with a total analysis time of 10 min the peak capacity increased from 200 calculated for a ^{T}LC system to 600 in ^{T}LC×^{T}LC, and 38,500 for the ^{X}LC×^{X}LC×^{T}LC system. It should be noted that in practice, the gain in peak capacity when moving from 1D-^{T}LC to spatial 3D-LC may be lower depending of the orthogonality of the retention mechanisms applied. The degree of orthogonality is influenced by the analyte properties, stationary-phase chemistries, and also the mobile-phase conditions used.

When using a fractal 3D-flow distributor, different design constrictions had to be taken into account, affecting the position of the Pareto-optimal front. The number of outlets in the 3D flow distributor equals the number of 3D channels, according to an even power of 2, *e.g.* $2^8 = 256$ outlets. Since the 3D flow distributor is designed to distribute flow over a square area, the length of the ^{1}D and ^{2}D channels should be equal. Furthermore, the number of ^{2}D channels corresponds to the square root of the number of 3D flow distributor outlets. For instance, 256

3D flow-distributor outlets imply the use of 16 parallel ^{2}D channels with 16 through holes (evenly) spaced across the ^{2}D channel. Fig. 5 shows the Pareto-optimal front of the spatial prototype device as depicted in Fig. 1, with fixed channel length while optimizing the operating pressure up to a maximum of 2 MPa. This front is different from the front obtained in Fig. 4, in which the pressure was kept fixed, while the lengths were optimized. The proposed $^{\mathrm{X}}$LC×$^{\mathrm{X}}$LC×$^{\mathrm{T}}$LC microfluidic device has the potential to yield a peak capacity of 8,100 in an analysis time of 11.5 minutes, assuming the use of orthogonal retention mechanisms operated in gradient mode. The performance of the prototype microfluidic 3D-LC device can be significantly improved by increasing the number of discrete channels in the second and third dimension. The dotted line in Fig. 5 depicts the Pareto-optimal front for a spatial 3D-LC device containing 32 ^{2}D channels and 1024 ^{3}D columns. This device would allow to generate a peak capacity of 23,000 within the same time period, which corresponds to a 3-fold increase in peak capacity.

5. Conclusions and perspectives

Spatial 3D-LC has the potential to yield unmatched peak capacities and peak-production rates compared to contemporary 1D- and 2D-LC strategies, given the fact that the total peak capacity is (ideally) the product of the three individual peak capacities and parallel ^{2}D and ^{3}D developments are realized. This makes spatial 3D-LC technology potentially suitable for high-throughput screening of a multitude of complex samples.

To create orthogonal retention mechanisms in the subsequent developments, a combination of isoelectric focusing (IEF) followed by two subsequent reversed-phase separations at high and low pH is envisioned. This can be achieved using a single monolithic stationary phases present in the ^{2}D and ^{3}D channels, as described in the current study. Alternatively, photografting approaches could be applied to functionalize the surface chemistry at the surface at a predetermined location using photomasks. In this way, ion-exchange (IEX) functionalities may be incorporated in the ^{2}D channels, while the ^{3}D would feature a RP gradient separation. A combination of IEF×IEX×RP would allow focusing of the analytes between the different developments, enhancing the detection sensitivity while the channel configuration, *i.e.*, combination of column lengths and i.d. applied, becomes less critical since “injection” band-broadening effects in each dimension becomes absent.

The application of mass-spectrometric detection techniques is mandatory in a proteomics setting. Therefore, a prototype 3D-LC chip was proposed that allows the elution of the analytes out of the separation body (^{X}LC×^{X}LC×^{T}LC). Analytes can then be detected in the effluent by using a “printing” method in pre-defined intervals, followed by the use of an imaging technique such as MS, to obtain a three-dimensional image of how the components leave the separation body over time. However, even when state-of-the-art MS imaging techniques are employed, the MS analysis of the numerous “prints” may become the time-limiting step. To exploit the full potential of spatial 3D-LC decreasing the MS time is mandatory. Hence, the success of spatial 3D-LC will partly depend on new developments in the field of MS technology, such as frequency tripled solid-state lasers with high pulse-repetition rates.[20]

6. Acknowledgements

BW acknowledges the Institute for Promotion of Innovation through Science and Technology in Flanders (IWT-Flanders) for a research grant. Support of this work by grants of the Research Foundation Flanders (G.0919.09 and G.0.103.11.N.10), the EUREKA framework (C2322.0227), and Thermo Fisher Scientific is gratefully acknowledged.

7. References

1. R. Aebersold, M. Mann, Mass spectrometry-based proteomics, *Nature*, 2003, **422**, 198-207.
2. S. Pan, R. Aebersold, R. Chen, J. Rush, D.R. Godlett, M.W. McIntosh, J. Zhang, T.A. Brentnall, Mass spectrometry based targeted protein quantification: methods and applications, *J. Proteome Res*. 2009, **8**, 787-797.
3. N. Rifai, M.A. Gillette, S.A. Carr, Protein biomarker discovery and validation: the long and uncertain path to clinical utility. *Nat. Biotechnol.* 2006, **24**, 971-983.
4. M. Tyers, M. Mann, From genomics to proteomics, *Nature*, 2003, **422**, 193-197.
5. J.C. Giddings, Two-dimensional separations: concept and promise, *Anal. Chem*. 1984, **56**, 1258A-1260A.
6. A.W. Moore, J.W. Jorgenson, Comprehensive three-dimensional separation of peptides using size-exclusion chromatography/reversed-phase liquid chromatography/optically gated zone electrophoresis, *Anal. Chem.* 1995, **67**, 3456-3463.

7. E. Davydova, P.J. Schoenmakers, G. Vivo-Truyols, Study on the performance of different types of three-dimensional chromatographic systems, *J. Chromatogr. A*, 2013, **1271**, 137-143.
8. G. Guiochon, N. Marchetti, K. Mriziq, R.A. Shalliker, Implementations of two-dimensional liquid chromatography, *J. Chromatogr. A* 2008, **1189**, 109-168.
9. L.D. Massart, B.G.M. Vandeginste, L.M.C. Buydens, S. de Jong, P.J. Lewi, J. Smeyers-Verbeke, Handbook of Chemometrics and Qualimetrics: Part A, Elsevier, Amsterdam, The Netherlands, 1997.
10. S. Eeltink, W.M.C. Decrop, G.P. Rozing, P.J. Schoenmakers, W.T. Kok, Comparison of the efficiency of microparticulate and monolithic capillary columns, *J. Sep. Sci.*, 2004, **27**, 1431-1440.
11. J.W. Dolan, L.R. Snyder, N.M. Djordjevic, D.W. Hill, T.J. Waeghe, Reversed-phase liquid chromatographic separation of complex samples by optimizing temperature and gradient time I. Peak capacity limitations, *J. Chromatogr. A*, 1999, **857**, 1-20.
12. A. Vaast, E. Tyteca, G. Desmet, P.J. Schoenmakers, S. Eeltink, Gradient-elution parameters in capillary liquid chromatography for high-speed separations of peptides and intact proteins, *J. Chromatogr. A*, 2014, **1355**, 149-157.
13. G. Guiochon, L.A. Beaver, M.F. Gonnord, A.M. Siouffi, M. Zakaria, Theoretical investigation of the potentialities of the use of a multidimensional column in chromatography, J. Chromatogr. 1983, 255, 415-437.
14. D.A Mair, E. Geiger, A.P. Pisano, J.M.J. Fréchet, F. Svec, Injection molded microfluidic chips featuring integrated interconnects, *Lab Chip*, 2006, **6** 1346-1354.
15. B. Wouters, J. De Vos, G. Desmet, H. Terryn, P.J. Schoenmakers, S. Eeltink, Design of a microfluidic device for comprehensive spatial two-dimensional liquid chromatography, *J. Sep. Sci.* 2015, **38**, 1123-1129.
16. C.D. Murray, The physiological principle of minimum work, *Proc. Natl. Acad. Sci. USA*, 1926, *12*, 207–214.
17. I. Rodriguez-Iturbe, A. Rinaldo Fractal River Basins, Cambridge University Press, UK, 1997.
18. D. Tondeur, L. Luo, Design and scaling laws of ramified fluid distributors by the constructal approach, *Chem. Eng. Sci.*, 2004, **59**, 1799-1813.
19. S. Eeltink, S. Dolman, F. Detobel, G. Desmet, R. Swart, M. Ursem, 1 mm ID poly(styrene-*co*-divinylbenzene) monolithic columns for high-peak capacity one- and

two-dimensional liquid chromatographic separations of intact proteins, *J. Sep. Sci.*, 2009, **32**, 2504-2509.

20. M.M. Gessel, J.L. Norris, R.M. Caprioli, MALDI imaging mass spectrometry: spatial molecular analysis to enable a new age of discovery, *J. Proteomics* 2014, **107**, 71-82.

FIGURE CAPTIONS

Figure 1. The spatial 3D-LC device consists of 3 modules. (A) shows the top module featuring the fractal 3D flow distributor (1), (B) shows the center module featuring 256 ‘downcomers’ (2) and the ^{1}D separation channel (3). (C) shows the bottom module featuring the ^{2}D flow distributor (4), ^{2}D separation channels (5), the flow collector (6), and 256 parallel ^{3}D channels (7). (D) shows a photograph of the assembled spatial 3D-LC device. The arrows represent the three subsequent developments in the X, Y, and Z direction, respectively.

Figure 2. (A) Photograph of a cross section of the microfluidic chip along its length. A monolithic stationary phase has been created *in-situ* in the channels of the 3D flow distributor and ‘downcomers’, 2D flow distributor and collector, parallel ^{2}D channels and the array of ^{3}D channels. (B) depicts physical barriers to confine the flow during the ^{1}D development, for the sake of clarity, an empty chip was sectioned for this purpose. Note: the physical barrier appears to be asymmetrical, which is caused by the presence of the final row of diamond-shaped pillars of the 2D flow distributor. Nomenclature as in Figure 1. (C) shows a SEM image of the bottom of a ^{3}D channel sectioned in half. (D) illustrates attachment to the channel wall. (E) a higher magnification showing the microglobule size.

Figure 3. Fractal 3D distribution of a red dye. (A) shows the distribution patterns after 5 generations of T-bifurbications and (B) after 8 successive generations yielding 256 outlets.

Figure 4. Pareto fronts for the optimization of the total peak capacity and analysis of one-dimensional ^{T}LC (dotted line), two-dimensional (coupled-column) ^{T}LC×TLC system (dashed line) operated at a maximum pressure of 100 MPa, and spatial three-dimensional ^{X}LC×^{X}LC×^{T}LC (solid line) operated at a maximum pressure of 2 MPa. Other parameters for calculations are defined in Table I.

Figure 5. Pareto fronts for the proposed ^{X}LC×^{X}LC×^{T}LC microfluidic device containing 16 ^{2}D channels and 256 ^{3}D channels and fixed channel lengths (full line) and spatial chip containing 32 ^{2}D channels and 1024 ^{3}D channels (dotted line). Operating pressure was varied between 0 and 2 MPa, other parameters for calculations are defined in Table I.

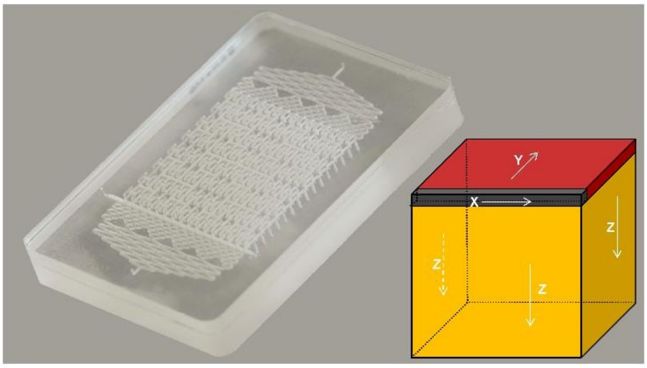

For TOC only

Spatial three-dimensional (3D-)LC is based on a novel concept and potentially offers unprecedented resolving power.

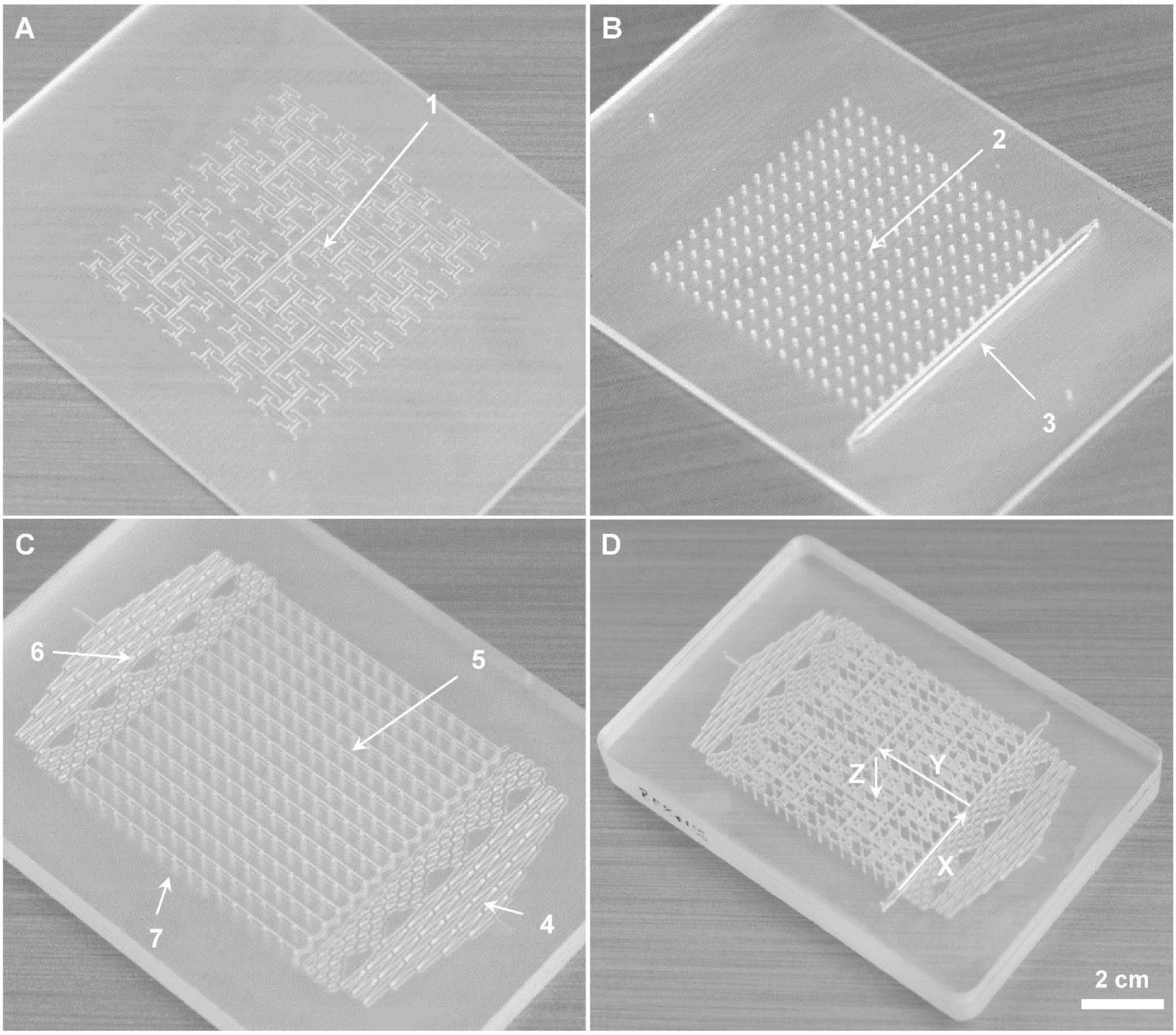

429

430 Figure 1

431

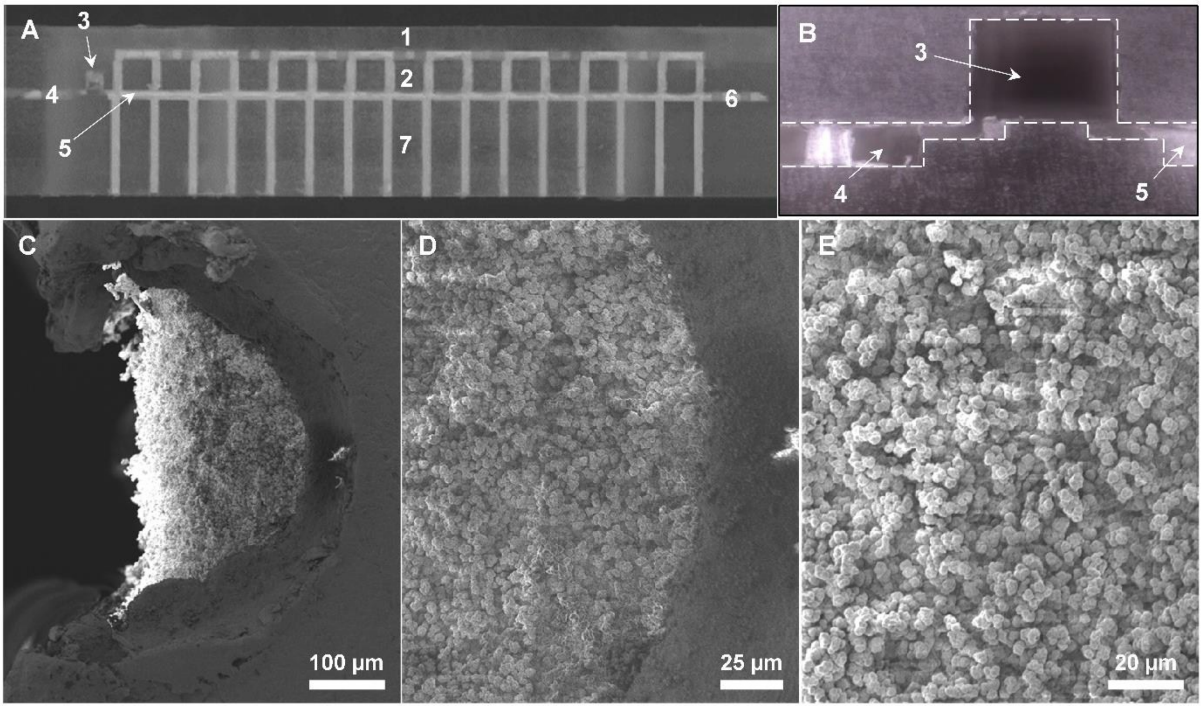

Figure 2

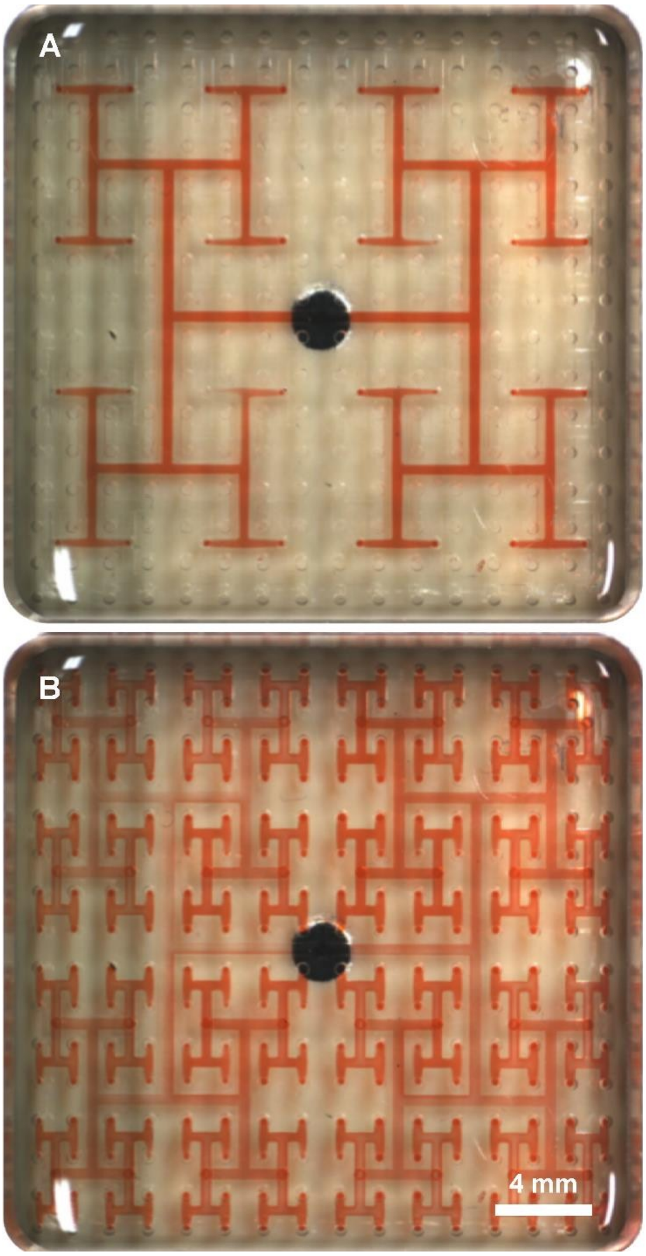

435

436 Figure 3

437

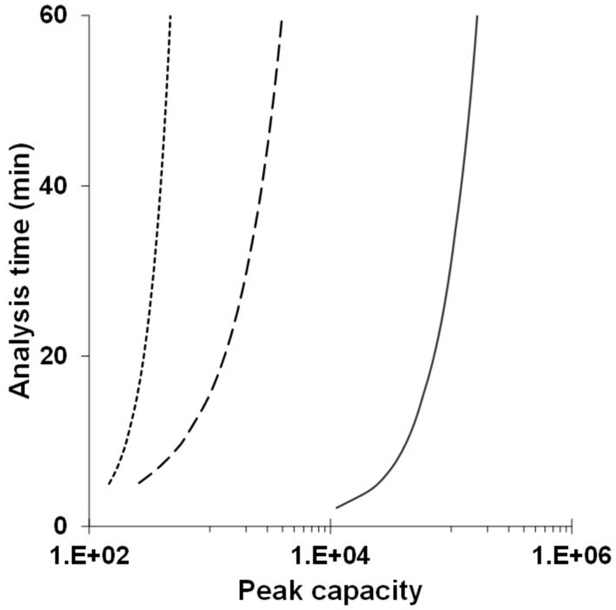

Figure 4

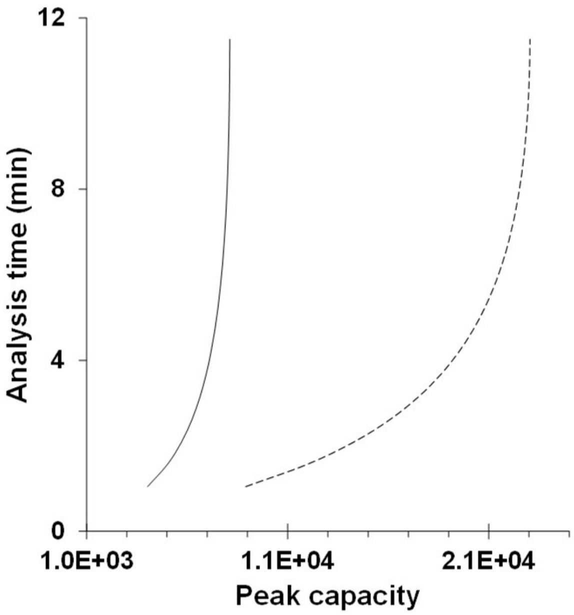

Figure 5